WIND TUNNEL VIRTUAL FLIGHT TEST FOR A TRANSPORT AIRCRAFT WITH SIMULATED ICE SHAPE

Linliang GUO*, Minghong ZHU*, Jian GUAN*, Bowen NIE*
***China Aerodynamics Research and Development Centre**

Keywords: *wind tunnel, virtual flight test, dynamically similarity, ice accretion*

Abstract

Ice build-up results in significant changes to the aerodynamics of the flying vehicle. This degrades the performance and controllability of the aircraft. The ice tolerant control system has been designed implemented to identify degradations in airplane performance and flying qualities resulting from ice contamination[1].Wind tunnel virtual flight test provide a method to assess and validate control system in the wind tunnel. It is intended that control system design incorporating icing issues can be conducted earlier into the design cycle to reduce the overall aircraft procurement time and risk[2-4], but also to validate the physical control circuit. This paper details a 3-degree-of-freedom (DOF) gimbaled mechanism to connect a model with simulated ice shape to a vertical support strut, the simulation results show that the attitude of the vehicle is stable and controllable.

1 Aerodynamic Effect Test of Simulated Ice Shape

1.1 Test Method

The test was carried out in Φ3.2m wind tunnel of China Aerodynamics Research and Development Centre, the test speed selected for this investigation set at about 15～35m/s. The wind tunnel is a closed circuit wind tunnel with a round test section of 3.2m diameter. The maximum free stream velocity achievable in the test section is approximately 115m/s, and the turbulence intensity is less than 2%.

The test model is supported by abdominal bracing (see Fig. 1), and the change of the angle of attack and sideslip of the model is realized by supporting device and turntable mechanism. The aerodynamic force of the model is measured by the strain gauge placed inside the model. The angle of attack is measured by the real-time tilt sensor, and the sensor is installed in internal level surface of the model. The sideslip angle is obtained by the nominal value of the turntable mechanism. The control surface deflection of the model is realized by the electromechanical actuator, and five electromechanical actuator controls two slices of elevator, two slices of aileron and one rudder respectively. The aircraft model is a carbon fiber dynamic similarity model at 1:20, and the specific parameters are shown in Table 1. The test wind speed ranges from 15m/s to 35m/s; the test angle of attack is -10 to 20 degrees, and the sideslip angle is -15 to 15 degrees.

Fig. 1. The photo of force measurement test

Table 1 Main parameters of the aircraft model

Model parameter	Value
Mass(kg)	13.16
Reference area(m^2)	0.31
Mean aerodynamic chord length(m)	0.2075
Length of the fuselage(m)	1.910
Wing span(m)	1.705
Distance from the c.g. to the tip of the nose(m)	0.8585
Deflection range of elevator (°)	-25～25
Deflection range of rudder (°)	-30～30
Deflection range of aileron (°)	-25～25

1.2 Simulated Ice Shape

The medium and severe simulated ice models located at the leading edge of the wing and the leading edge of the horizontal tail were obtained by Computational Fluid Dynamics (CFD) calculation (Fig. 2 and 3). After the ice shape was made into ice models at 1:20, the width and thickness were 2.5/1, 5/2, 5/3 and 10/6 (unit: mm) respectively. Because the shape was irregular, and each part of the ice type was divided into three sections for the convenience of processing. It is processed by 3D printing with acrylonitrile-butadiene-styrene (ABS) plastic. The installation of heavy icing shape on the model is shown in Fig. 4 and 5.

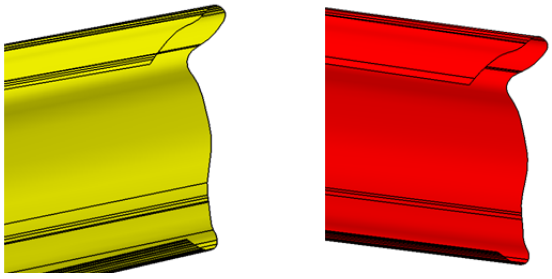

a. Medium ice accretion b. Severe ice accretion

Fig. 2. Artificial ice shape for wing

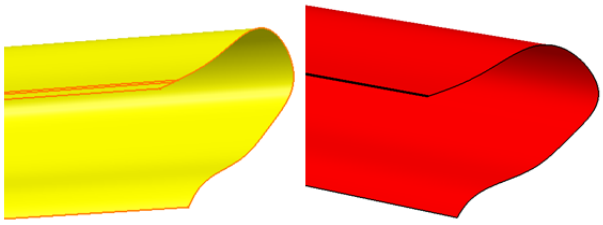

a. Medium ice accretion b. Severe ice accretion

Fig. 3. Artificial ice shape for horizontal tail

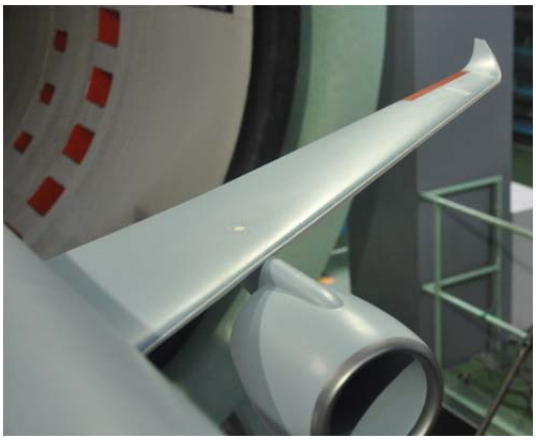

Fig. 4. Photos of the severe ice shape on the wing

Fig. 5. Photos of the severe ice shape on horizontal tail

1.3 Analysis of Aerodynamic Characteristics

1.3.1 Longitudinal and lateral aerodynamic characteristics

When the sideslip angle is 0 degrees, the longitudinal aerodynamic characteristic curves of different configurations are shown in Fig. 6. The stall characteristic of the aircraft is good, and the lift coefficient does not decrease sharply after the stall of angle of attack, and the lift coefficient increases with the increase of the angle of attack after the stall. The ice shape made the stall of angle of attack reduced. The stall occurs at an angle of attack of 11.5 degrees for clean configuration, while the stalling angle of attack is at 11 degrees and 9 degrees respectively for moderate ice and severe ice shape.

The drag coefficient is increased by freezing. The ice shape has a great influence on the lift-drag ratio, and makes the optimal lift drag ratio decreased. The maximum lift-drag ratio of the clean configuration is about 10, the

corresponding angle of attack is 6 degrees, the maximum lift-drag ratio of moderate ice accretion is about 8, the corresponding angle of attack is 5.5 degrees, the maximum lift-drag ratio of severe ice accretion is about 6.5, and the corresponding angle of attack is 5 degrees.

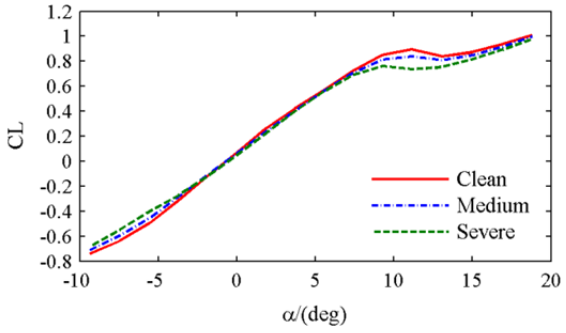

a. CL-α

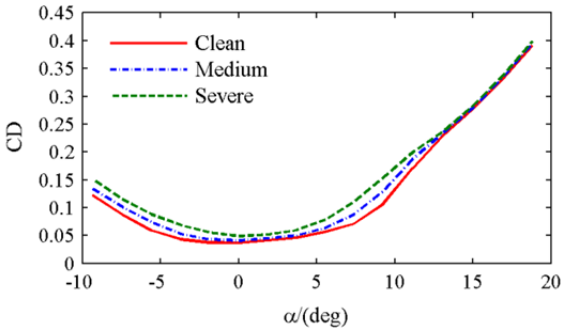

b. CD-α

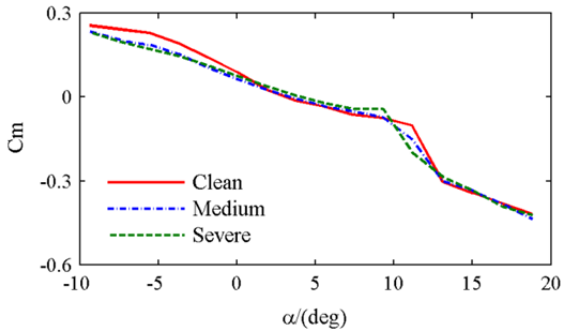

c. Cm-α

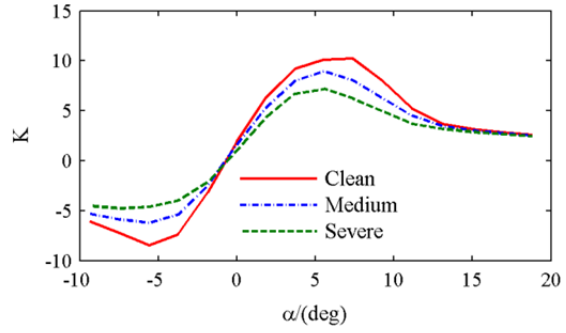

d. K-α

Fig. 6. Variation of longitudinal aerodynamic coefficients with angle of attack (β=0°)

Fig. 7 shows the lateral and directional aerodynamic characteristic under the wind velocity of 35m/s and sideslip angle of 6 degree. For the clean configuration, $C_{Y\beta}$=-0.02057, $C_{n\beta}$ =0.00344, $C_{l\beta}$=-0.00333. And for the moderate ice shape configuration, $C_{Y\beta}$ =-0.02049, $C_{n\beta}$ =0.00341, $C_{l\beta}$=-0.00302. The results show that the lateral stability is slightly weakened by ice shape, and the influence on the other lateral aerodynamic parameters is not obvious.

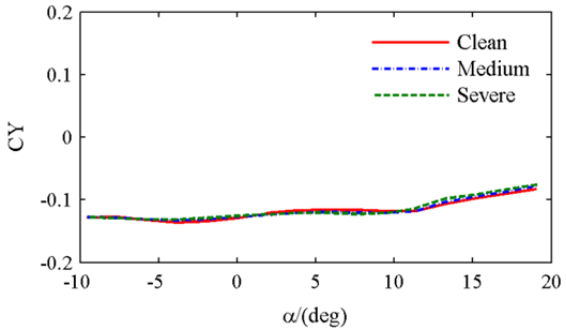

a. CY-α

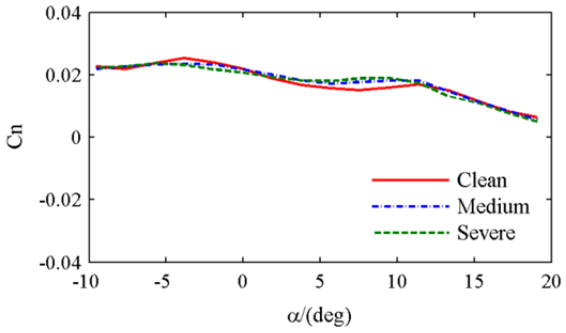

b. Cn-α

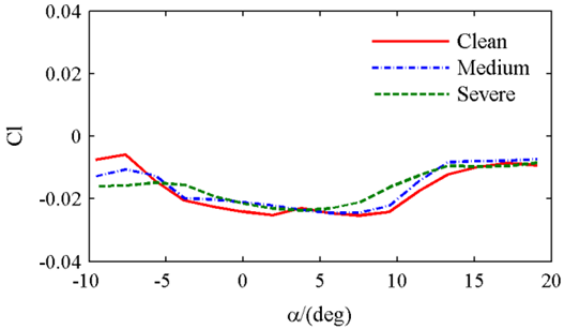

c. Cl-α

Fig. 7. Variation of lateral aerodynamic coefficients with angle of attack (β=6°)

1.3.2 Control surfaces efficiency

As shown in Fig. 8~10, it can be seen from the curve that the efficiency of the elevator, rudder and aileron decreases rapidly above the stall of angle of attack. The aileron efficiency is

relatively high at the range of ±5 degrees angle of attack. The ice effect on the aileron efficiency is greater than the elevator and rudder, the aileron efficiency is reduced by 20% at 5 degrees angle of attack under the severe icing condition. And the yaw moment produced by the aileron is small.

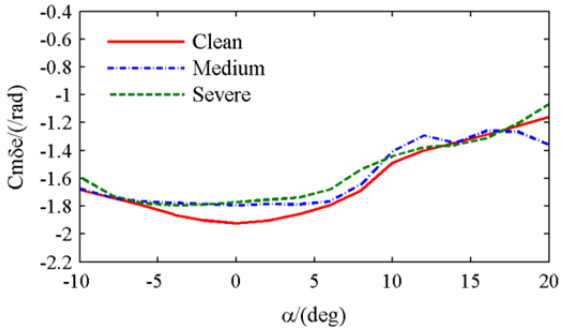

Fig. 8. Comparison of the elevator efficiency

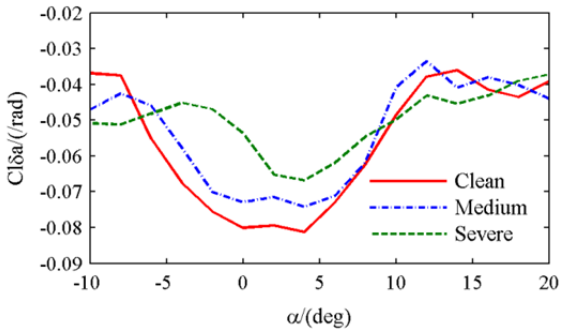

a. Clδa-α

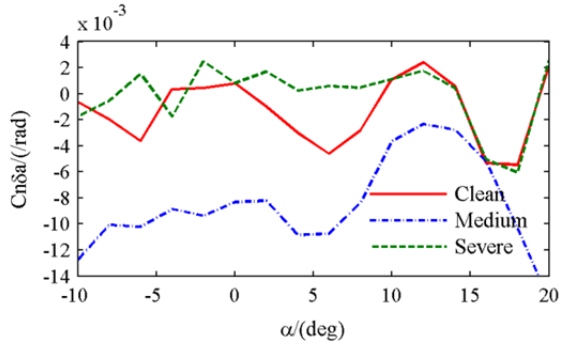

b. Cnδa -α

Fig. 9. Comparison of the aileron efficiency

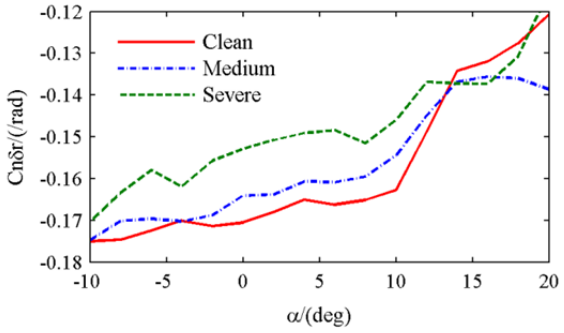

a. Cnδr-α

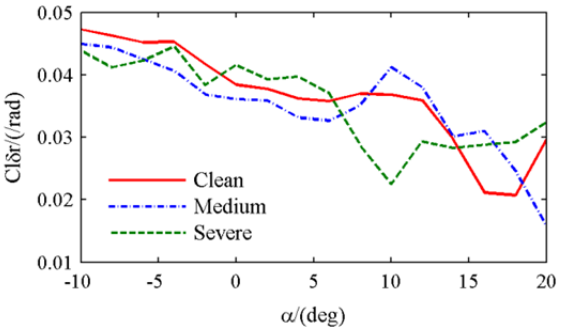

b. Clδr -α

Fig. 10. Comparison of the rudder efficiency

2 Experimental Setup of Virtual Flight Test

2.1 Support System

A three degree-of-freedom gimbal, ventrally installed in the model, is used in conjunction with an actively controlled model. Additionally, the gimbal is mounted on a vertical support strut which is fixed to the wind tunnel floor, as shown in Fig. 11. The ball gimbal with low mechanical clearance contributes small rolling friction force. The pendular angle is limited to 45°. The gimbal is shown in Fig. 12.

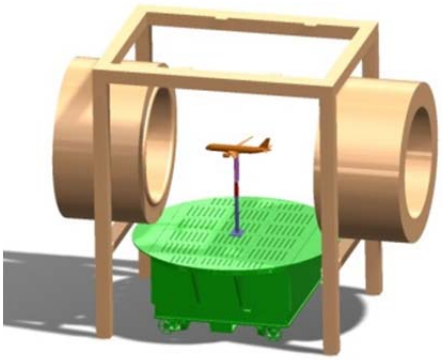

Fig. 11. Schematic of 3-DOF support system

Fig. 12. 3-DOF gimbal

2.2 Test Model

The virtual flight test used the same model as the force measurement test. Two cases of moderate and severe icing were simulated for the leading edge of both wing and horizontal tail. The model was mostly constructed of carbon fiber and the wing was made of carbon fiber-polyurethane foam sandwich structure. The inertial measurement unit (IMU), embedded computer and the servo-actuators were mounted in the model. The mass characteristics, center of gravity, and moment of inertia parameter used for the model can be adjusted through the counterweights installed at different places in the model.

2.3 Instrumentation and Hardware

The embedded computer, IMU and the actuators constitute flight control hardware platform. The angular rate signal is transmitted to the embedded computer as the control law inputs through RS-422 serial port. The control actuators commands, which are the primary outputs of control law, drive the deflection of the control surfaces through RS-485 serial port. The bandwidth of IMU is 50Hz, and the measurement range of the angular rate is 300°/s. The real-time Single-Board RIO is adopted as flight control computer. Control law execution, the attitude acquisition and the actuator drive are implemented in the field programmable gate array (FPGA) environment to insure real-time control. The maximum torque of the digital actuator is 3.5 N·m, and the maximum rate is 250°/s.

3 Design and Simulation of Control Law

3.1 Logic Design of Task Management

According to the process of the three degree of freedom dynamic wind tunnel test, the control law is divided into the following five stages:

1) The test preparation stage. After the flight control computer is powered on, it enters the test preparation phase. At this stage, the following items need to be completed: gyro and accelerometer calibration, check all of the control surfaces ensuring polarity correctness and normal work.

2) The wind tunnel starting stage. At this stage, the wind speed gradually increases and the control surfaces efficiency increases gradually. In the design of control law, the control surfaces should be prevented from saturation, and the control surfaces permissions should be released gradually with the increase of wind speed until full permissions.

3) The stable stage of wind speed. This stage is the task execution stage. In order to perform the task conveniently, the control law can respond to five kinds of flight modes: autonomous attitude control mode, autonomous angular velocity control mode, artificial attitude control mode, artificial angular velocity control mode and override operation mode. The autonomous angular velocity control mode is designed to realize flight quality identification.

4) The wind stopping stage. At this stage, the wind speed gradually decreases and the control surfaces efficiency decreases gradually. In the design of control law, the control surfaces should be prevented from saturation, and The authority of the control surfaces should be reduced gradually with the decrease of wind speed until the control surfaces are locked.

5) The end stage. At this stage, the test has been completed, the control surfaces are locked, the operator stores data, and the flight control computer is powered down.

3.2 Analysis of Typical Handling

From the analysis of above data, the simulated ice shape has little effect on the aerodynamic characteristics. Therefore, only the clean configuration and the severe icing configuration are analyzed. The response of two configurations under longitudinal and lateral directional square waves is shown in Fig. 13. The simulated test lasted for 90s, and the control mode was override control mode, that is, the manual operation was added to the autonomous attitude control mode. The test process is: the joystick and the control surfaces is checked during 1s～10s, the test start switch is pressed at 12 second, wind tunnel starts operation at 15 second, the override control switch is open at 28

second, the pitching pulse signal input occurs at 30 second, the rolling pulse signal input occurs at 40 second, the yawing pulse signal input occurs at 50 second, wind tunnel stops running at 60 second, and the test ends at 90 second.

In the test, the pitching angle command is given at 5 degrees. After the operation of the wind tunnel, the model starts to pitch up slowly. With the increase of wind speed, the authority of the control surfaces is gradually released, and the control surfaces are completely released at 15m/s speed. The pitch motion of the model accelerates and reaches the desired attitude angle quickly. After the attitude is stable, the elevator has a 0.4 degree shift between the clean configuration and the severe ice state, and the pitch rate peak value of the clean configuration is slightly higher, which is related to the reduction of the efficiency of the elevator after the ice accretion. After rolling operation, the roll rate of the clean configuration is slightly larger about 0.5 degree /s, and the aileron deflection is slightly smaller. After the directional control, the yaw rate and the sideslip angle of the clean configuration are slightly larger, while the sideslip brings obvious lateral movement and small pitch motion. Generally speaking, the simulated ice shape has little effect on the dynamic response characteristics of the model.

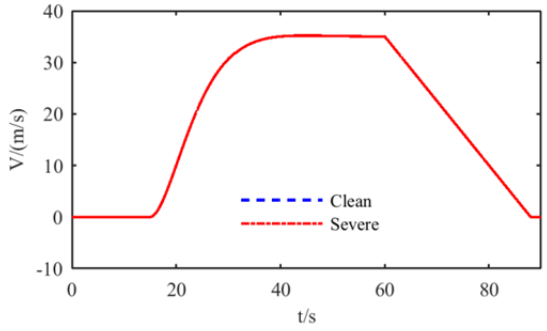

a. Wind velocity

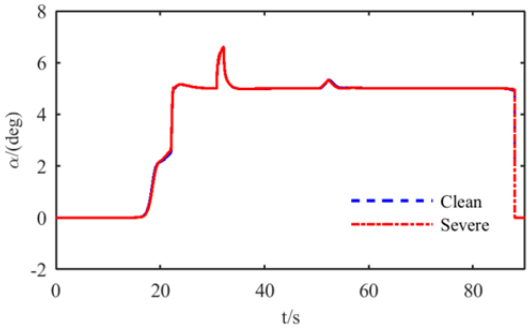

b. Angle of attack

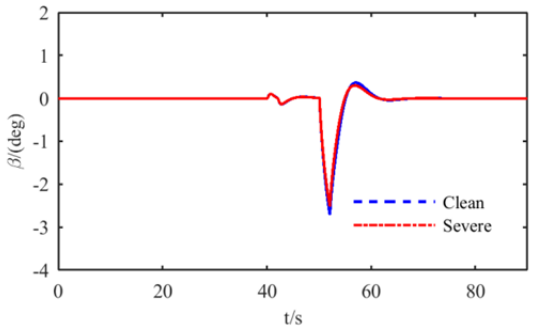

c. Sideslip angle

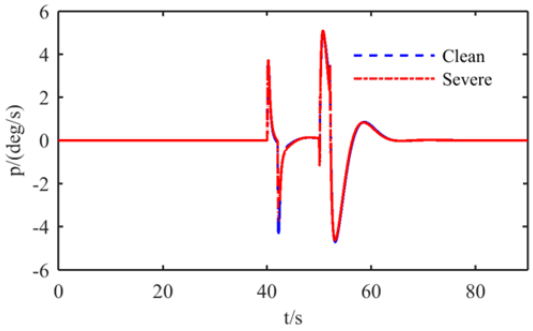

d. Rolling rate

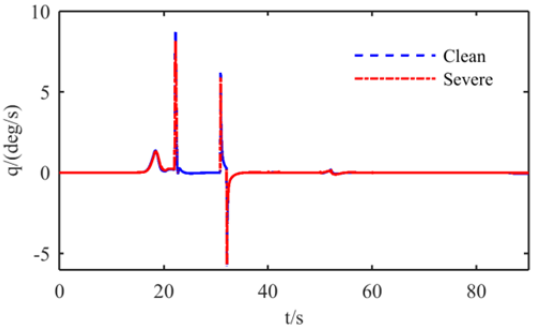

e. Pitching rate

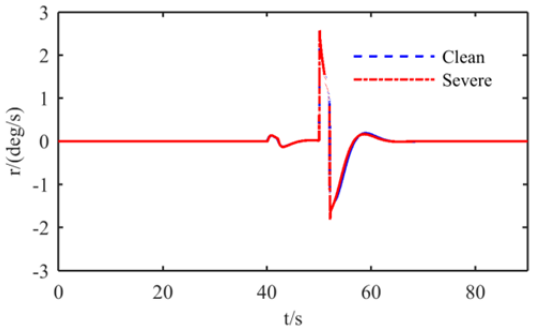

f. Yawing rate

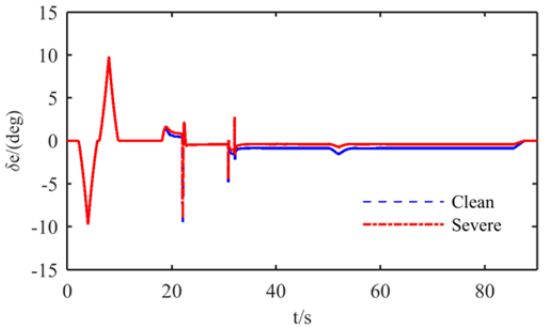

g. Deflection of elevator

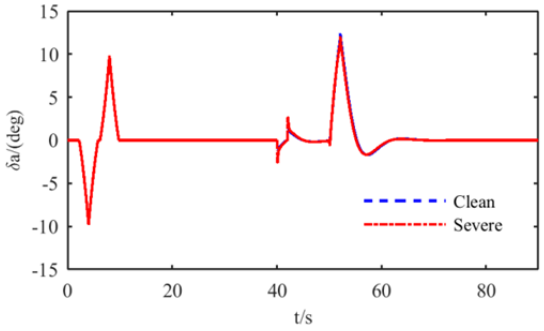

h. Deflection of aileron

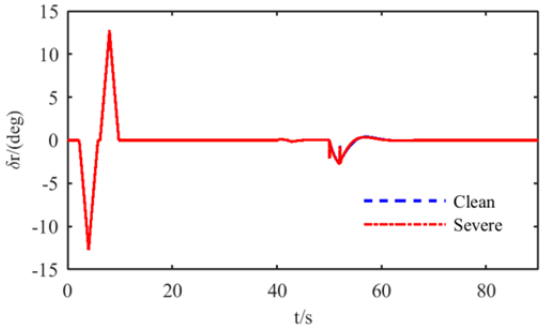

i. Deflection of rudder

Fig. 13. Response results of longitudinal and lateral handling under different ice shape

4 Conclusions

Through the above research, the main conclusions are as follows:

1) The stall attack of angle and maximum lift-drag ratio decreases in turn for clean configuration, moderate icing and severe icing configuration.

2) The elevator, rudder and aileron efficiency decreases rapidly above the stall angle of attack. The ice accretion has a greater influence on the aileron efficiency than the elevator and rudder.

3) The whole process control of the three degree of freedom test is effective, ensuring safe and efficient operation and stability and control characteristics research. The influence of ice shape on the dynamic response characteristics of the aircraft model coincides with the basic aerodynamic characteristics obtained from the force measurement test.

References

[1] David R. Gingras and Billy P. Barnhart. Development and Implementation of a Model Driven Envelope Protection System for In-Flight Ice Contamination. AIAA 2010-8141.

[2] Arpita Sen, Niteen P. Bhange, Dr. Pankaj Wahi and Dr. A. K. Ghosh. 5-Degree-of-Freedom Dynamic Rig for Wind Tunnel Test of Aerospace Vehicles. AIAA 2009-5605.

[3] J. Pattinson and M. H. Lowenberg. A Multi-Degree-of-Freedom Rig for the Wind Tunnel Determination of Dynamic Data. AIAA 2009-5727.

[4] A. Gatto and M. H. Lowenberg. Evaluation of a Three-Degree-of-Freedom Test Rig for Stability Derivative Estimation. Journal of Aircraft, Vol.43, No.6, 2006.11

Contact Author Email Address

guolinliangliang@163.com

Copyright Statement

The authors confirm that they, and/or their company or organization, hold copyright on all of the original material included in this paper. The authors also confirm that they have obtained permission, from the copyright holder of any third party material included in this paper, to publish it as part of their paper. The authors confirm that they give permission, or have obtained permission from the copyright holder of this paper, for the publication and distribution of this paper as part of the ICAS proceedings or as individual off-prints from the proceedings.